Far-Field Optical Imaging of a Linear Array of Coupled Gold Nanocubes: Direct Visualization of Dark Plasmon Propagating Modes

Hung-Ying Chen,[†,▽] Chieh-Lun He,[‡,▽] Chun-Yuan Wang,[†] Meng-Hsien Lin,[‡] Daisuke Mitsui,[§] Miharu Eguchi,[§] Toshiharu Teranishi,[⊥,∥,*] and Shangjr Gwo[†,‡,*]

[†]Department of Physics and [‡]Institute of Nanoengineering and Microsystems, National Tsing-Hua University, Hsinchu 30013, Taiwan, [§]Department of Chemistry, Graduate School of Pure and Applied Sciences, University of Tsukuba, 1-1-1 Tennodai, Tsukuba, Ibaraki 305-8571, Japan, [⊥]Institute for Chemical Research, Kyoto University, Gokasho, Uji, Kyoto 611-0011, Japan, and [∥]CREST, Japan Science and Technology Agency (JST), 1-1-1 Tennodai, Tsukuba, Ibaraki 305-8571, Japan. [▽] These author contributed equally to this work.

ABSTRACT Plasmonic nanoantenna arrays hold great promise for diffraction-unlimited light localization, confinement, and transport. Here, we report on linear plasmonic nanoantenna arrays composed of colloidal gold nanocubes precisely assembled using a nanomanipulation technique. In particular, we show the direct evidence of dark propagating modes in the plasmon coupling regime, allowing for transport of guided plasmon waves without far-field radiation losses. Additionally, we demonstrate the possibility of plasmon dispersion engineering in coupled gold nanocube chains. By assembling a nanocube chain with two sections of coupled nanocubes of different intercube separations, we are able to produce the effect of a band-pass nanofilter.

KEYWORDS: dark plasmon mode · nanoantenna array · gold nanocube · plasmon coupling

The diffraction laws in optics limit the spatial resolution of light focusing and guiding by conventional lenses, fibers, and waveguides to about the light wavelength. This is in sharp contrast to the operation of antennas in the radiowave and microwave regimes, where subwavelength confinement of electromagnetic energies is a common practice. Recently, the concept of optical nanoantennas based on plasmonic metal nanostructures has emerged as a promising route to realize optics and photonics far beyond the diffraction limit.[1−4] In its inception, plasmonic nanoantennas composed of single metallic nanorods or nanoparticles were proposed as subwavelength receivers and/or transmitters of optical fields.[5,6] Subsequently, metallic gap nanoantennas in the coupled (closely spaced) geometries of bow-tie,[7] end-to-end nanorod pair,[8,9] and nanoparticle dimer[10] were introduced to enhance the radiation intensity and efficiency. Very recently, linear nanoparticle array antennas (similar to the case of Yagi-Uda antennas[11]) have been proposed and demonstrated for high directionality in the far-field radiation.[12−14] Furthermore, a novel optical nanospectrometer has been proposed by utilizing these arrays to distribute different frequency contents of the emitter radiation into chosen spatial locations or directions.[15] These recent results indicate that linear nanoparticle array antennas are indeed a promising approach for deep-subwavelength light confinement and transport.

To perform localization and guiding of light in plasmonic metal nanostructures, the major concerns are related to internal and external losses in these metal nanostructures. The internal losses are mostly related to the resistive (ohmic) damping (electron−electron scattering, electron−phonon scattering, *etc.*) and scattering at surfaces, roughness, or defects of metal nanostructures. On the other hand, the radiative damping results in most of the external losses.[16−18] To overcome the internal losses, one approach is to utilize high-quality, crystalline metal nanostructures, such as noble metal nanowires[19,20] and nanoparticles[21,22] synthesized by chemical methods. On the other hand, the radiative damping can be prevented by taking advantage of the dark modes for plasmon excitation and propagation in strongly coupled metal nanostructures.[23−29] To generate the conditions of strong plasmon coupling for metal nanoparticles, a facile self-assembly technique has been applied to prepare branched chain networks of close-packed metal nanoparticles.[30] However, precisely

* Address correspondence to gwo@mx.nthu.edu.tw, teranisi@scl.kyoto-u.ac.jp.

Received for review July 31, 2011 and accepted September 6, 2011.

Published online September 06, 2011
10.1021/nn2029007

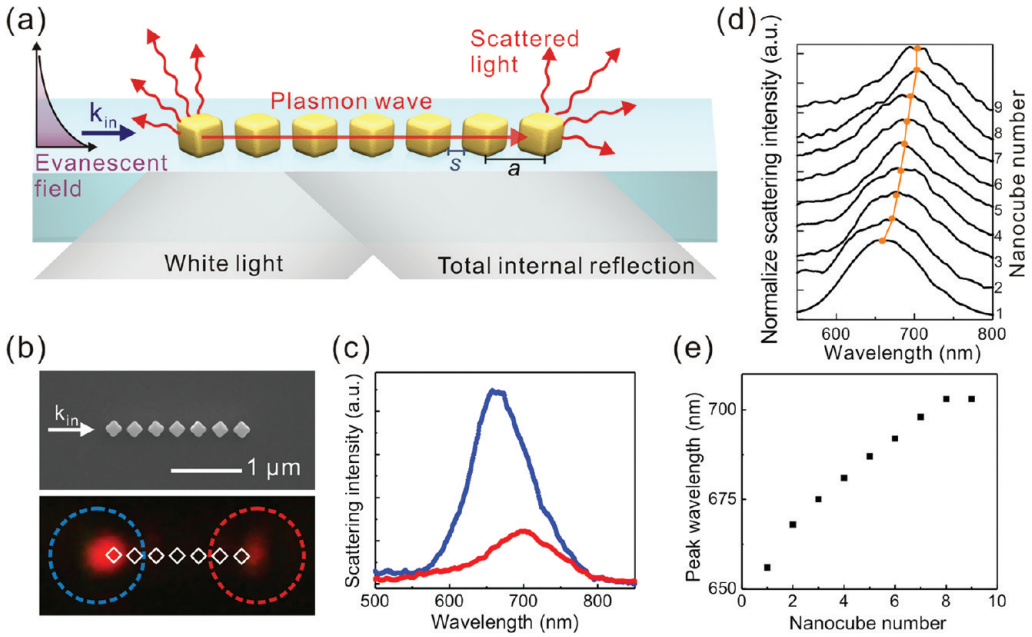

Figure 1. (a) Schematic of the optical scattering measurement setup in ambient air. (b) FE-SEM image showing a chain composed of 7 uniformly spaced nanocubes (intercube tip-to-tip separation: 70 ± 5 nm). Under the near-field plasmon coupling conditions, the resonant scattering signals (in the red spectral region) only appear at the incident and distal ends of the chain. The incident light direction is directed parallel to the chain, and the collected light passes through a polarizer parallel to the chain axis (longitudinal direction). (c) Scattering spectra acquired at both ends of the chain [regions marked by the dashed circles in corresponding colors in (b)]. (d) Measured scattering spectra for the distal ends of the chains with different numbers of nanocubes and the same intercube spacing. (e) Resonant peak wavelength *vs* the number of nanocubes in the chains.

controlling the coupling strength and configuration is still very difficult. In this aspect, a more demanding version of template-assisted self-assembly[31,32] might be required for such tasks. Recently, we have developed an alternative nanomanipulation technique for assembly of gold octahedron nanocrystal dimers with precisely controlled interoctahedron nanogaps.[28] Here, by studying the gold nanocube chains precisely assembled with tunable intercube separations, the fundamental plasmonic effects can be revealed in detail under well-prepared experimental settings, such as the number and spacing of nanocubes as well as the incident light direction and scattering light polarization. This approach could open the door to future proof-of-concept experiments for discovering novel plasmon coupling effects.

RESULTS AND DISCUSSION

Far-Field Optical Imaging. We utilized chemically prepared gold nanocubes with a well-defined crystal structure as well as monodispersed size and shape. Large and uniform gold nanocubes (169 ± 7.0 nm in side length) were synthesized by a two-step seed-mediated growth method.[33] The gold nanocubes were randomly deposited onto indium tin oxide (ITO)-coated quartz substrates using a drop casting technique. Subsequently, the nanocubes were assembled into tip-to-tip chains in a field-emission scanning electron microscope (FE-SEM) using an *in situ* four-probe manipulator. By using this nanomanipulation technique, we can obtain one-by-one assembled nanocube chains on ITO-coated quartz substrates with well-separated individual nanocubes, exact nanocube number, and precisely controlled lattice periodicity (*a*) intercube separation (*s*) (see Figure 1a). We assembled nanocube chains with the tip-to-tip geometry for two practical reasons. First, the tip-to-tip nanocube chains have a simple plasmon coupling geometry, which is advantageous for the analysis of coupling modes. Second, this type of structure has a well-defined separation between neighboring nanocubes.

Schematic representation of the optical scattering measurement setup in ambient air is shown in Figure 1a. Samples to be measured were placed in an optical evanescent field produced by total internal reflection (TIR) of light (from a 100 W halogen lamp or a supercontinuum laser) using a prism glass. In addition, the incident light direction was aligned to be parallel to the chain, and the scattered light was collected through a polarizer parallel to the chain axis (longitudinal polarization). This polarization is chosen because it can be related to the plasmon guiding mode, which propagates toward the distal end of the chain.[19]

Figure 1b shows an FE-SEM image and a corresponding optical scattering image taken for a chain composed of 7 uniformly spaced nanocubes (intercube tip-to-tip separation $s \approx 70$ nm). The positions of nanocubes are also schematically displayed in the optical

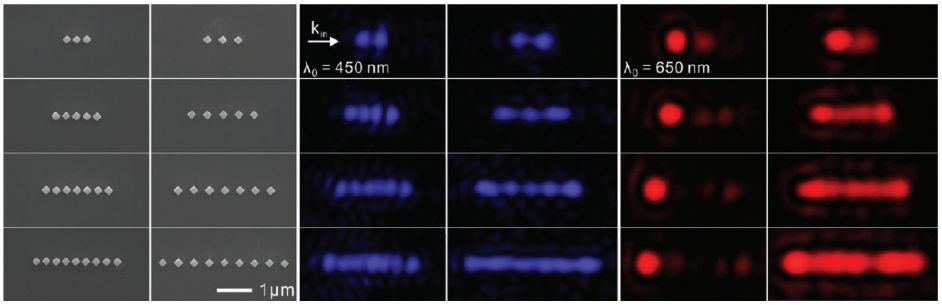

Figure 2. FE-SEM and optical scattering images of plasmon-coupled (intercube tip-to-tip separation: 70 ± 5 nm) and uncoupled (without plasmon coupling; intercube tip-to-tip separation: 210 ± 8 nm) nanocube chains composed of 3, 5, 7, and 9 uniformly spaced nanocubes at varying incident laser wavelengths. It should be noted that the plasmon guiding modes only occur for coupled chains at a resonant wavelength (650 nm).

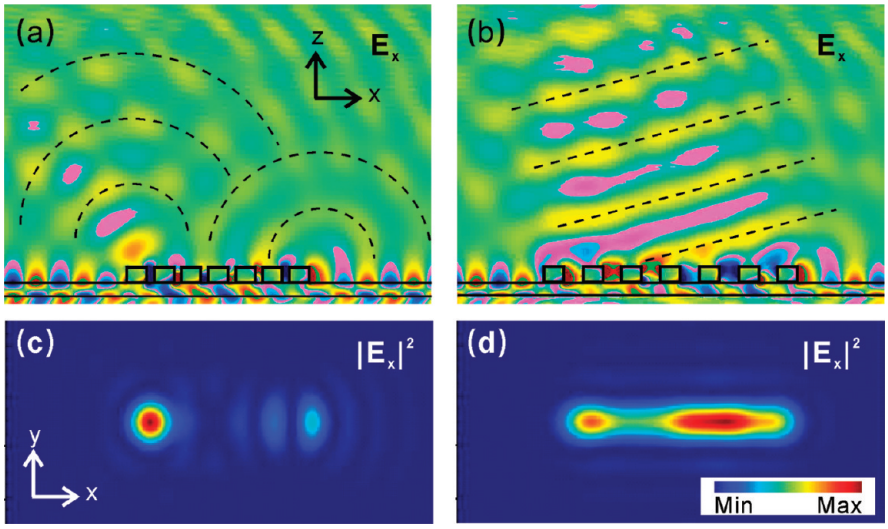

Figure 3. FDTD simulation results of optical scattering from two kinds of nanocube chains under plasmon resonant conditions. Two videos showing the detailed scattering and coupling processes are included in Supporting Information. Screenshots from the videos show electric-field patterns in cross-sectional view (a) for a plasmon-coupled chain with an intercube separation of 70 nm, and (b) for an uncoupled (without plasmon coupling) chain with an intercube separation of 210 nm. The dashed lines depict the wavefronts, which propagate to the far-field. (c,d) Simulated far-field images obtained from (a) and (b), respectively. FDTD simulation parameters are described in Methods.

scattering image. Under near-field plasmon coupling conditions, we can clearly observe the occurrence of the dark plasmon propagating mode inside the chain, which exhibits no far-field radiation (therefore, free from the effects of radiative damping). For chains with different numbers of nanocubes, optical scattering images using nonresonant and resonant laser lights are shown in Figure 2.

It is noteworthy that the resonant scattering signals (in the red spectral region) only appear at the incident and distal ends of the chain, indicating a waveguiding effect. Similar to the case of plasmon waveguiding and propagation on silver colloidal nanowires,[34] far-field light absorption/re-emission from one-dimensional (1D) plasmonic nanostructures is confined to two chain ends due to the strongly bound plasmon field and the requirement of momentum matching between incoming/scattered photons and propagating plasmons in 1D metal nanostructures. The requirement of momentum matching is relaxed only at nanostructure discontinuities (sites with broken symmetry). Our observation is also consistent with the previous suggestion that plasmonic nanoparticle chains are nanoscale receivers and concentrators of unfocused light analogous to multiple-element radio wave antennas, such as Yagi-Uda antennas.[35]

Figure 1c shows the scattering spectra taken from both ends of the chain, corresponding to regions marked by dashed circles in corresponding colors in Figure 1b. For the distal chain end (red curve), the resonant peak is red-shifted about 40 nm compared to that of the incident end (blue curve) of the chain. Figure 1d presents the measured scattering spectra for the distal ends of the chains with different numbers of nanocubes and at the same intercube spacing. A plot of the resonant peak wavelength *versus* the number of nanocubes in the chains is displayed in Figure 1e, which shows an increasing red shift with increasing number of nanocubes. The red shift starts to

saturate after a critical chain length (*i.e.*, a certain number of nanocubes). This is in agreement with the dispersion relations of propagating plasmon waves confined in metal nanoparticle chains theoretically studied by other groups.[36,37]

Finite-Difference Time-Domain (FDTD) Simulations. Figure 3 shows the 3-D simulation results performed by the FDTD method for coupled and uncoupled chains composed of 7 uniformly spaced gold nanocubes with intercube separation of 70 nm (Figure 3a,c) and 210 nm (Figure 3b, d), respectively. The incident light is under plasmon resonant conditions. Here, we show both the vertical cross sections of electric-field (E_x) patterns (Figure 3a,b; screenshots of the video included in Supporting Information) and simulated far-field images (Figure 3c,d). The depicted wavefronts in Figure 3a reveal that the far-field radiation originates from two point sources at the incident and distal ends of the plasmon-coupled chain. Inside this chain, the incident light is converted to a confined plasmon wave propagating along the chain direction (see details in the video included in Supporting Information). On the contrary, the incident light can be scattered into the far-field by the uncoupled chain, as shown in Figure 3b. The scattered light from the uncoupled chain exhibits different fringe patterns, which can be adjusted by changing the incident light wavevector. A video showing the detailed scattering and far-field propagating processes can also be found in Supporting Information. In addition, according to the simulated electric-field distributions, strong near-fields locate around gold nanocubes, independent of the intercube separation. Thus, the most appropriate way to identify the presence of a dark plasmon mode is far-field optical imaging. In Figure 3c,d, the simulated far-field images confirm that the experimental observation of a dark plasmon propagating mode critically depends on the distance of intercube separation.

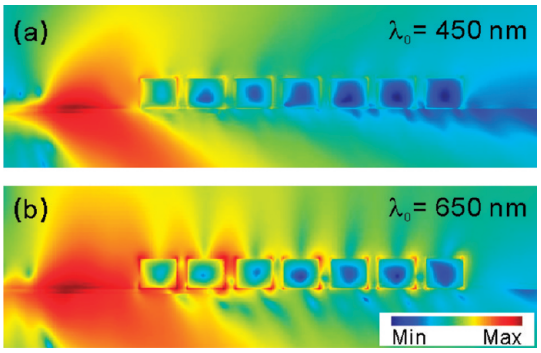

Figure 4. FDTD simulation results of optical scattering from plasmon-coupled nanocube chain (intercube separation: 70 nm) under local excitation. The excitation light is located at the left end of the chain and restricted to within a diameter of 100 nm. The intensity patterns in cross-sectional view correspond to local light excitations (a) at a nonresonant wavelength (450 nm) and (b) at a resonant wavelength (650 nm).

To confirm the plasmon waveguiding effect, we have also performed a FDTD study using our experimental parameters. Figure 4 shows the FDTD simulation results for light scattering from a plasmon-coupled chain under local excitation at a nonresonant wavelength of 450 nm (Figure 4a) and at a resonant wavelength of 650 nm (Figure 4b). As shown in

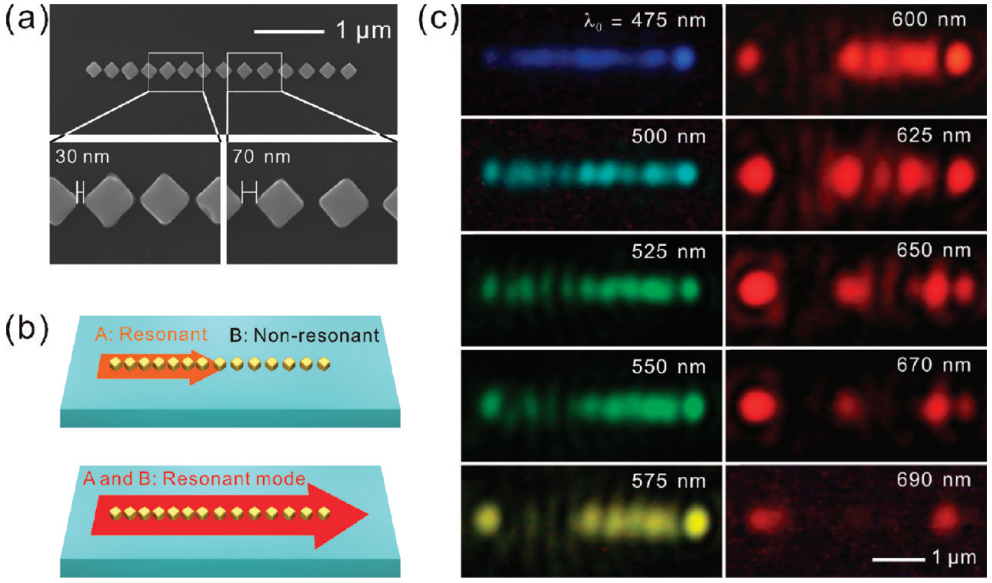

Figure 5. (a) FE-SEM images of a nanocube chain partitioned into two sections, A and B, with different tip-to-tip separations. To form the A/B chain for the present study, two different tip-to-tip separations of 30 nm (LHS) and 70 nm (RHS) were adopted during nanocube chain assembly. (b) Schematic drawings of the A/B chain, which are resonant or nonresonant at different incident laser wavelengths. (c) Optical scattering images of the A/B chain for the incident laser wavelengths at 475, 500, 525, 550, 575, 600, 625, 650, 670, and 690 nm. The laser incident angle is 55°, and a polarizer parallel to the chain axis is used to collect the scattered light. The complete A/B chain is nonresonant at 475–550 nm and resonant at 670–690 nm. At 550–650 nm, only the LHS section is at resonance.

Figure 4a, under nonresonant excitation conditions, light would not propagate along the chain but would be scattered out or reflected. In contrast, as shown in Figure 4b (under resonant excitation conditions), light propagates toward the distal end of the chain. This simulation result can also be used to explain the far-field optical images shown in Figure 2, where the incident TIR light excites the whole chain. Under these conditions, the gold nanocubes behave as individual light scattering centers and the grating effect plays an important role in resulting images. More experimental results of scattering images under nonresonant conditions can be found in Figures S4 and S5 in Supporting Information.

A/B Plasmonic Chain Served as 1D Optical Band-Pass Filter. In our measurements, we find that both the number and spacing of nanocubes are important parameters to manipulate the plasmon dispersion relations in the plasmon-coupled chains. On this basis, we demonstrated the important feature of plasmon dispersion engineering by precise controlling of intercube spacing. Figure 5a shows FE-SEM images of a nanocube chain partitioned into two sections, A and B, with different tip-to-tip separations. To form the A/B chain for the present study, two different tip-to-tip separations of 30 nm (left-hand side, LHS) and 70 nm (right-hand side, RHS) were adopted during nanocube chain assembly. It should be noted that both separations are within the plasmon coupling range. In Figure 5b, we show the schematic representations of the A/B chain which are partially resonant or totally resonant at different incident laser wavelengths due to the difference in dispersion bandwidths of chain sections A and B. Figure 5c shows optical scattering images of the A/B chain for the incident laser wavelengths at 475−690 nm. To acquire these images, the laser incident angle was set at 55° and a polarizer parallel to the chain axis was used to collect the scattered light. These images show that the complete length of the A/B chain is nonresonant at 475−550 nm and resonant at 650−690 nm. At the resonance wavelength, the scattering into far-field photons only occurs at the ends of the chain. As a result, electromagnetic energy can be guided below the diffraction limit along the length of a closely spaced gold nanocube chain, converting the optical field into nonradiating surface plasmons. In contrast, at 550−650 nm, only the LHS section is resonant and we have a partially resonant case. For excitation at 670 nm, we find a localization of the scattered light at the middle of the chain, indicating that this photon energy corresponds to the interface mode energy of the A/B chain. This result presents the direct experimental evidence for controlled energy transport along plasmonic waveguides by plasmon dispersion engineering. Especially, we show that 1D optical band-pass filter can be formed at a designable wavelength region (in this case, ~670−690 nm) by choosing suitable intercube separations.

CONCLUSIONS

In summary, size- and shaped-controlled gold nanocubes have been successfully applied to assemble high-quality gold nanocube chains. Using these chains, we are able to measure the dispersion relations of coupled plasmons with respect to the number of composing nanocubes and the intercube distance. In contrast to the existing results in the literature, we find that the plasmon coupling in gold nanocrystal structures can extend over a long spatial range (a few micrometers), resulting from the superior plasmonic properties of gold nanocubes. In addition, we confirm that plasmonic waveguiding can only occur when the intercube distance is very small (much smaller than the nanocube feature size; under near-field plasmon coupling conditions). Under these conditions, we demonstrate the important feature of plasmon dispersion engineering in gold nanocube chains. The results could have important implications for plasmonic waveguides, filters, and antennas operating beyond the diffraction limit.

METHODS

Synthesis of Large Au Nanocubes. Large Au nanocubes were synthesized by a two-step seed-mediated growth method.[33] The first seed Au nanocrystals were synthesized by swiftly adding 600 μL of ice-cold 10 mM $NaBH_4$ aqueous solution to 7.8 mL of an aqueous solution of cetyltrimethylammonium bromide (CTAB, 78 μmol) and $HAuCl_4 \cdot 4H_2O$ (2.5 μmol). The brownish solution containing ~4 nm Au nanocrystal solution was obtained after vigorously stirring for 2 min. The second Au nanocube seeds (side length: 43 nm) were synthesized by adding the ~4 nm seed solution to the growth solution, following the previous report. The growth solution was prepared by adding 600 μL of 0.1 M L-ascorbic acid aqueous solution to 4.8 mL of an aqueous solution of CTAB (80 μmol) and $HAuCl_4 \cdot 4H_2O$ (1.0 μmol) to form a colorless solution. A 2.5 μL portion of 10-fold diluted seed solution was introduced to the growth solution with slow stirring. Storing still at room temperature for 12 h gave the pale red solution containing Au nanocubes with edge size of 43 ± 1.9 nm (Figure S1a, Supporting Information, the second Au nanocube seeds) by the slow reduction of Au^+ to Au^0. The second Au nanocube seeds were purified by centrifugation. Subsequently, a 400 μL portion of the second seed solution was poured in 28 mL of another growth aqueous solution containing CTAB (800 μmol) and $HAuCl_4 \cdot 4H_2O$ (6.0 μmol) to which 3.6 mL of 0.1 M L-ascorbic acid aqueous solution was added. The large Au nanocubes with edge size of 169 ± 7.0 nm were formed after 1 day growth without stirring (Figure S1b). The concentration of second seed dispersion was controlled at 44, 20, 10, 5, and 2.3 μM so that the molar ratio to growth solution was changed. A spontaneous precipitation of these large Au nanocubes was used for purification.

Optical Measurement Setup. The chain sample was positioned onto a glass prism, and an index-matching silicone oil was placed between the sample and the prism. Scattering light was collected by an optical microscope with a 100× objective lens (Olympus MPLN, NA = 0.9) and a spectrometer (Ocean Optics, QE65000) (Figure S3). We recorded the scattering images using a color digital camera (Canon EOS 1000D).

FDTD Simulation Parameters. The finite-difference time-domain (FDTD) simulations[38] were performed with a commercial package (Lumerical FDTD solutions v.7.5) for plasmon-coupled and uncoupled gold nanocube chain systems. The gold nanocubes with a side length of 175 nm were placed on an ITO-coated (140 nm) silica substrate with a vacuum gap of 3 nm. The incident light was TM-polarized and with incident angle of 60° and wavelength of 700 nm. The dielectric functions of gold and ITO were adopted from the experimental data reported by Johnson and Christy[39] and Laux *et al.*,[40] respectively. The refractive index of silica was assumed to be 1.46. We used a non-uniform mesh volume with a minimum step size of 3 nm. The far-field images were obtained by simulating the light path through an optical microscope, where an objective lens (NA = 0.9) was used to collect the scattered light, and a lens was used to focus the collected light onto the display screen.

Acknowledgment. This work was supported in part by the National Science Council in Taiwan through the National Nanoscience and Nanotechnology Program under Grant No. NSC-99-2120-M-007-004 and Grant-in-Aid for Scientific Research on Priority Area "Strong Photon-Molecule Coupling Fields for Chemical Reactions" (No. 470) (19049007) from the MEXT, Japan.

Supporting Information Available: Synthesis and characterization of large Au nanocubes, optical measurement setup and additional optical characterization of Au nanocube chains, as well as supplemental video and legend. This material is available free of charge *via* the Internet at http://pubs.acs.org.

REFERENCES AND NOTES

1. Stockman, M. I. Nanoplasmonics: The Physics Behind the Applications. *Phys. Today* **2011**, *64*, 39–44.
2. Gramotnev, D. K.; Bozhevolnyi, S. I. Plasmonics beyond the Diffraction Limit. *Nat. Photonics* **2010**, *4*, 83–91.
3. Schuller, J. A.; Barnard, E. S.; Cai, W.; Jun, Y. C.; White, J. S.; Brongersma, M. L. Plasmonics for Extreme Light Concentration and Manipulation. *Nat. Mater.* **2010**, *9*, 193–204.
4. Novotny, L.; van Hulst, N. Antennas for Light. *Nat. Photonics* **2011**, *5*, 83–90.
5. Crozier, K. B.; Sundaramurthy, A.; Kino, G. S.; Quate, C. F. Optical Antennas: Resonators for Local Field Enhancement. *J. Appl. Phys.* **2003**, *94*, 4632–4642.
6. Novotny, L. Effective Wavelength Scaling for Optical Antennas. *Phys. Rev. Lett.* **2007**, *98*, 266802.
7. Schuck, P. J.; Fromm, D. P.; Sundaramurthy, A.; Kino, G. S.; Moerner, W. E. Improving the Mismatch between Light and Nanoscale Objects with Gold Bowtie Nanoantennas. *Phys. Rev. Lett.* **2005**, *94*, 017402.
8. Mühlschlegel, P.; Eisler, H.-J.; Martin, O. J. F.; Hecht, B.; Pohl, D. W. Resonant Optical Antennas. *Science* **2005**, *308*, 1607–1609.
9. Alù, A.; Engheta, N. Input Impedance, Nanocircuit Loading, and Radiation Tuning of Optical Nanoantennas. *Phys. Rev. Lett.* **2008**, *101*, 043901.
10. Alù, A.; Engheta, N. Hertzian Plasmonic Nanodimer as an Efficient Optical Nanoantenna. *Phys. Rev. B* **2008**, *78*, 195111.
11. Balanis, C. A. *Antenna Theory: Analysis and Design*, 3rd ed.; John Wiley & Sons: New York, 2005.
12. Li, J.; Salandrino, A.; Engheta, N. Shaping Light Beams in the Nanometer Scale: A Yagi-Uda Nanoantenna in the Optical Domain. *Phys. Rev. B* **2007**, *76*, 245403.
13. Kosako, T.; Kadoya, Y.; Hofmann, H. F. Directional Control of Light by a Nano-optical Yagi-Uda Antenna. *Nat. Photonics* **2010**, *4*, 312–315.
14. Curto, A. G.; Volpe, G.; Taminiau, T. H.; Kreuzer, M. P.; Quidant, R.; van Hulst, N. F. Unidirectional Emission of a Quantum Dot Coupled to a Nanoantenna. *Science* **2010**, *329*, 930–933.
15. Li, J.; Salandrino, A.; Engheta, N. Optical Spectrometer at the Nanoscale Using Optical Yagi-Uda Nanoantennas. *Phys. Rev. B* **2009**, *79*, 195104.
16. Link, S.; El-Sayed, M. A. Size and Temperature Dependence of the Plasmon Absorption of Colloidal Gold Nanoparticles. *J. Phys. Chem. B* **1999**, *103*, 4212–4217.
17. Sönnichsen, C.; Franzl, T.; Wilk, T.; von Plessen, G.; Feldmann, J. Plasmon Resonances in Large Noble-Metal Clusters. *New J. Phys.* **2002**, *4*, 93.1–93.8.
18. The plasmon damping process in noble metal nanoparticles is characterized by the decay constant T_2, which is related to both nonradiative decay (energetic relaxation or absorption *via* ohmic loss mechanisms) and radiative decay (scattering of an exciting electromagnetic wave by nanoparticles) channels. For large nanoparticles (>25 nm in diameter, see refs 16 and 17), the plasmon damping process is dominated by radiative decay. Since large Au nanocubes with edge size of 169 ± 7.0 nm were employed for our experiments, the far-field radiative damping is the most important issue for the reduction of energy loss in the studied plasmonic nanosystems.
19. Ditlbacher, H.; Hohenau, A.; Wagner, D.; Kreibig, U.; Rogers, M.; Hofer, F.; Aussenegg, F. R.; Krenn, J. R. Silver Nanowires as Surface Plasmon Resonators. *Phys. Rev. Lett.* **2005**, *95*, 257403.
20. Wei, H.; Ratchford, D.; Li, X.; Xu, H.; Shih, C.-K. Propagating Surface Plasmon Induced Photon Emission from Quantum Dots. *Nano Lett.* **2009**, *9*, 4168–4171.
21. Chen, C.-F.; Tzeng, S.-D.; Chen, H.-Y.; Lin, K.-J.; Gwo, S. Tunable Plasmonic Response from Alkanethiolate-Stabilized Gold Nanoparticle Superlattices: Evidence of Near-Field Coupling. *J. Am. Chem. Soc.* **2008**, *130*, 824–826.
22. Lin, M.-H.; Chen, H.-Y.; Gwo, S. Layer-by-Layer Assembly of Three-Dimensional Colloidal Supercrystals with Tunable Plasmonic Properties. *J. Am. Chem. Soc.* **2010**, *132*, 11259–11263.
23. Nordlander, P.; Oubre, C.; Prodan, E.; Li, K.; Stockman, M. I. Plasmon Hybridization in Nanoparticle Dimers. *Nano Lett.* **2004**, *4*, 899–903.
24. Halas, N. J.; Lal, S.; Chang, W.-S.; Link, S.; Nordlander, P. Plasmons in Strongly Coupled Metallic Nanostructures. *Chem. Rev.* **2011**, *111*, 3913–3961.
25. Liu, M.; Lee, T.-W.; Gray., S. K.; Guyot-Sionnest, P.; Pelton, M. Excitation of Dark Plasmons in Metal Nanoparticles by a Localized Emitter. *Phys. Rev. Lett.* **2009**, *102*, 107401.
26. Chu, M.-W.; Myroshnychenko, V.; Chen, C. H.; Deng, J.-P.; Mou, C.-Y.; de Abajo, F. J. G. Probing Bright and Dark Surface-Plasmon Modes in Individual and Coupled Noble Metal Nanoparticles Using an Electron Beam. *Nano Lett.* **2009**, *9*, 399–404.
27. Koh, A. L.; Bao, K.; Khan, I.; Smith, W. E.; Kothleltner, G.; Nordlander, P.; Maler, S. A.; McComb, D. W. Electron Energy-Loss Spectroscopy (EELS) of Surface Plasmons in Single Silver Nanoparticles and Dimers: Influence of Beam Damage and Mapping of Dark Modes. *ACS Nano* **2009**, *3*, 3015–3022.
28. Yang, S.-C.; Kobori, H.; He, C.-L.; Lin, M.-H.; Chen, H.-Y.; Li, C.; Kanehara, M.; Teranishi, T.; Gwo, S. Plasmon Hybridization in Individual Gold Nanocrystal Dimers: Direct Observation of Bright and Dark Modes. *Nano Lett.* **2010**, *10*, 632–637.
29. Huang, J.-S.; Kern, J.; Geisler, P.; Weinmann, P.; Kamp, M.; Forchel, A.; Biagioni, P.; Hecht, B. Mode Imaging and Selection in Strongly Coupled Nanoantennas. *Nano Lett.* **2010**, *10*, 2105–2110.
30. Lin, S.; Li, M.; Dujardin, E.; Girard, C.; Mann, S. One-Dimensional Plasmon Coupling by Facile Self-Assembly of Cold Nanoparticles into Branched Chain Networks. *Adv. Mater.* **2005**, *17*, 2553–2559.
31. Yin, Y.; Lu, Y.; Gates, B.; Xia, Y. Template-Assisted Self-Assembly: A Practical Route to Complex Aggregates of Monodispersed Colloids with Well-Defined Sizes, Shapes, and Structures. *J. Am. Chem. Soc.* **2001**, *123*, 8718–8729.

32. Rycenga, M.; Cobley, C. M.; Zeng, J.; Li, W.; Moran, C. H.; Zhang, Q.; Qin, D.; Xia, Y. Controlling the Synthesis and Assembly of Silver Nanostructures for Plasmonic Applications. *Chem. Rev.* **2011**, *111*, 3669–3712.
33. Sau, T. K.; Murphy, C. J. Room Temperature, High-Field Synthesis of Multiple Shapes of Gold Nanoparticles in Aqueous Solution. *J. Am. Chem. Soc.* **2004**, *126*, 8648–8649.
34. Sanders, A. W.; Routenberg, D. A.; Wiley, B. J.; Xia, Y.; Dufresne, E. R.; Reed, M. A. Observation of Plasmon Propagation, Redirection, and Fan-Out in Silver Nanowires. *Nano Lett.* **2006**, *6*, 1822–1826.
35. de Waele, R.; Koenderink, A. F.; Polman, A. Tunable Nanoscale Localization of Energy on Plasmon Particle Arrays. *Nano Lett.* **2007**, *7*, 2004–2008.
36. Koenderink, A. F.; Polman, A. Complex Response and Polariton-like Dispersion Splitting in Periodic Metal Nanoparticles Chains. *Phys. Rev. B* **2006**, *74*, 033402.
37. Fung, K. H.; Chan, C. T. Plasmonic Modes in Periodic Metal Nanoparticle Chains: A Direct Dynamic Eigenmode Analysis. *Opt. Lett.* **2007**, *32*, 973–975.
38. Taflove, A.; Hagness, S. C. *Computational Electrodynamics: The Finite-Difference Time-Domain Method*, 3rd ed.; Artech House: Boston, 2005.
39. Johnson, P. B.; Christy, R. W. Optical Constants of Noble Metals. *Phys. Rev. B* **1972**, *6*, 4370–4379.
40. Laux, S.; Kaiser, N.; Zoller, A.; Gotzelmann, R.; Lauth, H.; Bernitzki, H. Room-Temperature Deposition of Indium Tin Oxide Thin Films with Plasma Ion-Assisted Evaporation. *Thin Solid Films* **1998**, *335*, 1–5.